Journal of
Applied Remote Sensing

Assessing stream bank condition using airborne LiDAR and high spatial resolution image data in temperate semirural areas in Victoria, Australia

Kasper Johansen
James Grove
Robert Denham
Stuart Phinn

Assessing stream bank condition using airborne LiDAR and high spatial resolution image data in temperate semirural areas in Victoria, Australia

Kasper Johansen,[a,b,c] James Grove,[d] Robert Denham,[c] and Stuart Phinn[a,b]

[a]University of Queensland, Joint Remote Sensing Research Program, Biophysical Remote Sensing Group, Brisbane, Queensland 4072, Australia
k.johansen@uq.edu.au

[b]University of Queensland, School of Geography, Planning and Environmental Management, Centre for Spatial Environmental Research, Brisbane, Queensland 4072, Australia

[c]Ecosciences Precinct, Queensland Government, Remote Sensing Centre, Department of Science, Information Technology, Innovation and the Arts, 41 Boggo Road, Brisbane, Queensland 4102, Australia

[d]University of Melbourne, School of Resource Management and Geography, Parkville, Victoria 3010, Australia

Abstract. Stream bank condition is an important physical form indicator for streams related to the environmental condition of riparian corridors. This research developed and applied an approach for mapping bank condition from airborne light detection and ranging (LiDAR) and high-spatial resolution optical image data in a temperate forest/woodland/urban environment. Field observations of bank condition were related to LiDAR and optical image-derived variables, including bank slope, plant projective cover, bank-full width, valley confinement, bank height, bank top crenulation, and ground vegetation cover. Image-based variables, showing correlation with the field measurements of stream bank condition, were used as input to a cumulative logistic regression model to estimate and map bank condition. The highest correlation was achieved between field-assessed bank condition and image-derived average bank slope ($R^2 = 0.60$, $n = 41$), ground vegetation cover ($R^2 = 0.43$, $n = 41$), bank width/height ratio ($R^2 = 0.41$, $n = 41$), and valley confinement (producer's accuracy = 100%, $n = 9$). Cross-validation showed an average misclassification error of 0.95 from an ordinal scale from 0 to 4 using the developed model. This approach was developed to support the remotely sensed mapping of stream bank condition for 26,000 km of streams in Victoria, Australia, from 2010 to 2012. [DOI: 10.1117/1.JRS.7.073492]

Keywords: stream bank condition; airborne remote sensing; light detection and ranging; multispectral imagery; channel morphology; index of stream condition; riparian vegetation.

Paper 13083 received Mar. 18, 2013; revised manuscript received Oct. 2, 2013; accepted for publication Oct. 3, 2013; published online Oct. 28, 2013.

1 Introduction

Increasingly, river management is considered a holistic exercise, where isolated work at a reach scale is moving toward planning at catchment scales. This results in compromises between the spatial and temporal extent of information collected. In Europe, the Water Framework Directive has created the demand for assessment at a country and continent scale.[1] In Australia, the importance of water as an anthropogenic and environmental resource has resulted in mapping and monitoring of stream condition mainly at a state scale through field-based approaches.[2–4] Such snapshot approaches do not allow a quantification of riverbank erosion rates but only report condition, i.e., the morphology of riverbank relative to a reference state. Stream bank condition is one of the several parameters generally used for assessment of stream condition as it is related

0091-3286/2013/$25.00 © 2013 SPIE

to changes such as channel widening and incision caused by climatic and/or anthropogenic factors.[5]

Sediment supplied by bank erosion provides bed and suspended material to the channel. If these sediment inputs are above reference conditions, they may disturb ecological habitats and change the water chemistry by contributing nutrients or other adhered pollutants.[6] Knowing the stream bank condition and the associated extent and position of erosion in a catchment enables more effective river management and allows clearer comparison of river systems against each other for management prioritization.

1.1 *Field Approaches*

Field approaches focusing on mapping bank condition for managing catchments tend to be rapid and based on visual and quantitative assessment of the present form of stream channels.[7–12] More detailed analysis and larger field-based sampling density of bank stability are more data intensive[13] and hence tend to be limited to reach scale management of tens of kilometers of stream length. As field-based approaches are time consuming, they are generally used to sample selected stream sections. Therefore, the samples may, in some cases, not be a representative of large areas.[14] If sites are selected randomly, variation in bank condition cannot be tracked over time, except at fixed sentinel sites. Interoperator variability and subjective visual interpretation may compromise the accuracy of field observations.[15,16] The use of remotely sensed data has been identified as a suitable means to address the limitations of field-based approaches for assessment of riparian zones, including bank condition, as remotely sensed data can provide complete spatial coverage.[17]

1.2 *Remotely Sensed Approaches*

Remote sensing of the physical form of streams and their riparian zones have mainly relied upon high-spatial resolution optical and light detection and ranging (LiDAR) data because of the limited width of riparian zones, dense vegetation cover, and spatial scale of variability.[18–20] Winterbottom and Gilvear[21] used geomorphic bank variables as well as sediment type, floodplain vegetation, and flood magnitudes to predict bank erosion probability from multitemporal high-spatial resolution aerial photography. The results showed that accurate erosion probability mapping can be used for effective river management and predictions of the effects of flood regime changes. Several articles have also found multitemporal image data useful for identifying changes in stream and bank geomorphic characteristics.[18,22] Bank stability and bank condition have previously been mapped with some success in relatively homogenous natural tropical savanna riparian environments in the Northern Territory, Australia using the extent of bare ground and amount of canopy cover as explanatory variables mapped from high-spatial resolution satellite image data.[23]

Airborne LiDAR data are important for collecting information on stream banks and riparian vegetation due to its capability to capture three-dimensional information on vegetation and banks at very fine spatial scales.[20,24] Airborne LiDAR sensors derive information on the elevation and reflectance of terrain and vegetation from a pulse or continuous wave laser fired from an airborne transmitter, for which its position is precisely and accurately measured. Processing of the reflected LiDAR signal provides an accurate measure of distance between the transmitter and reflecting surfaces based on the time of travel of the pulse and the position of the sensor.[24] Airborne LiDAR data can produce very detailed digital elevation and terrain models.[25] Milan et al.[26] stated that digital elevation models (DEMs) can be used for estimation of scour and fill for sediment budgets within fluvial environments. A large number of fluvial terrain and hydraulic modeling studies have successfully used airborne LiDAR data,[27–30] whereas others have used multitemporal LiDAR data and DEM differencing to detect geomorphic changes within streams.[31] Casas et al.[32] successfully assessed levee stability of the Sacramento River using airborne LiDAR data to map levee crown width, height, and water and landside slopes to produce a levee stability index. Tarolli et al.[33] asserted that with the high levels of geomorphic detail derivable from high-resolution and high-quality airborne and terrestrial laser scanners, there is a need for developing methods for mapping channel networks, bank geometry,

slope, and erosion scars. Some studies have also highlighted the benefits of combining airborne LiDAR data with high-spatial resolution optical image data to improve the mapping of riparian zone and physical form of biophysical characteristics.[34,35] Multitemporal coverage of LiDAR and optical image data, before and after a catastrophic flood, allowed erosion volumes and the relative contributions from different erosion processes to be quantified along a 100-km stretch of the Lockyer Creek in Queensland, Australia.[36,37] The combination of LiDAR and optical data was found essential for feature delineation and subsequent process interpretation.

1.3 *Index of Stream Condition*

In the State of Victoria, Australia, the original Index of Stream Condition (ISC) was designed to provide information on the condition of lowland rivers at the state scale.[2] It consisted of a subindex for physical form with the following components: (1) bank stability, (2) bed stability, (3) fish barriers, and (4) woody debris. These physical form indicators were included to provide key information on the ecological condition of Victorian streams. They were also recognized as indicators that could be reliably measured in the field by trained Catchment Management Authority staff. The bank erosion indicator was based on a comparison with photographic examples and a brief description of five levels of erosion. The types of erosion included in the examples consisted of both fluvial entrainment and mass failures, but were mainly tailored to common situations found in Victoria, such as erosion signatures left by incision and subsequent channel widening.[38] Photographs allowed the assessor to identify key geomorphic features, such as breaks in slope and the lack of vegetation cover, which indicated whether erosion may have occurred in the past. So, while this method was tested and found to be objective and repeatable,[2] with low variability between different observers, it was not quantitative in terms of areas, volumes, rates, and processes of erosion.

In Australia, it is often very difficult to assess the timing of the last erosion, due to the high interannual variability in rainfall and flows and sparse flow data.[39] To accommodate this issue, a reference condition of no erosion was used. Any erosion that was identified recently, however, reduced the condition score as it would lower the stream bank stability. The condition was scored at three 30-m long transects within each site with the average reported for the site. Sites were randomly selected and were aggregated to provide information at the reach scale, typically varying from 5 to 40 km in length. In 2004, the second statewide ISC assessment included a modified bank condition indicator, which incorporated some proxy measures of reference condition.[10] For example, bank condition was not assessed on the outside of meander bends, where erosion is expected to occur in the majority of cases.[40] Therefore, the outside of a meander should not necessarily be scored poorly. Also, the bank was defined more clearly by describing the concept of a bank-full channel, giving examples of terraced and confined channels, so that the correct active bank could be assessed. To obtain complete spatial coverage and enable effective future monitoring of ISC indicators, including bank condition, the third statewide ISC assessment initiated in 2010 was based on analysis of airborne LiDAR and high-spatial resolution optical image data. This research presents the method developed for the third statewide ISC assessment for measuring bank condition.

1.4 *Objective*

Currently, no suitable methods exist for mapping bank condition over large spatial extents (>100 km of stream length). Remote sensing is the only appropriate means for large spatial extent mapping of riparian areas.[15] However, only datasets providing high levels of details and information on landform and vegetation characteristics are suitable because of the varying spatial scales of stream banks.[19,41] Therefore, the objective of this research was to develop and apply an approach for mapping bank condition from airborne LiDAR and high-spatial resolution optical image data to allow the existing ISC method to be implemented with complete spatial coverage for large spatial extents. This addresses a significant gap in knowledge for stream and riparian zone assessment and management-related activities.

2 Study Area and Data

2.1 *Study Area*

The spatial extent of the study area covered parts of the natural water courses forming the Werribee catchment area (Fig. 1). The Werribee River is the major drainage stream emanating from the Werribee catchment, and the study area included the Lerderderg River and Pyrites, Parwan, and Djerriwarrh Creek tributaries. The main flow direction is south from the hilly Ordovician slate, shale, siltstone, and sandstone formation in the northern part of the study area until reaching basalts at the confluence with the Werribee River,[42] where flows turn east and then southeast before eventually draining into Port Phillip Bay. The southern half of the study area is a part of the flat Victorian Volcanic Plain bioregion.[43] The southern plain is characterized by anthropologically modified terrain with agricultural (grazing and cultivation) and urban land use. Being close to Melbourne, the land use is dominated by semirural residential style allotments. The southern parts of the study area also have small scale quarry and coal mining activities. The streams, riparian zones, and associated floodplains of this part of the Werribee catchment have been significantly modified by these anthropogenic activities and flow regulation from dams and weirs. The study area within the Werribee catchment receives 500 to 600 mm of rain annually, which is evenly distributed throughout the year.[44] Discharges of the Werribee River within the study area vary considerably with average monthly flows from 0 to 1415 ml/day (average monthly flow of 54 ml/day) recorded between 1978 and 2011 at the Bacchus March Station.[45]

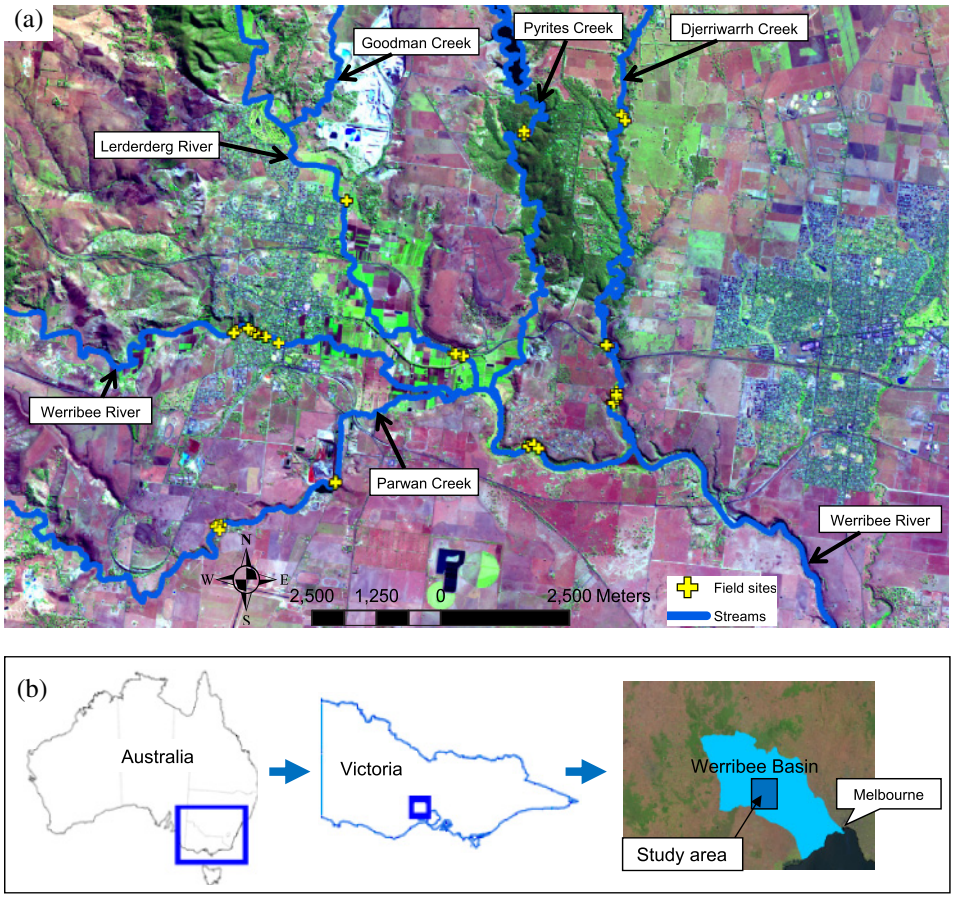

Fig. 1 (a) Area and stream sections covered by the LiDAR and Ultracam-D image data in (b) the Werribee catchment, Victoria, Australia. Fifty field plots were assessed.

2.2 *Field Approach and Data*

Field plots of set dimensions introduce difficulties for categorizing a stream bank section into a score of bank condition because of variation in bank condition within the sections.[23,46] Hence, it was decided to assess bank condition in the field within homogenous plots to ensure that bank condition scores did not vary at the plot level for those areas related to the image data. In this case, a homogenous field plot was defined as an area of the bank with similar biophysical vegetation and physical form characteristics and no obvious variation in the previous, field-derived, ISC bank condition. A number of both quantitative and qualitative measurements (Table 1) were obtained within each of the 50 homogenous plots assessed in the field between October 24 and 28, 2009, to facilitate the interpretation of the research results. These plots generally measured between 8 and 20 m in length parallel to the stream and 3 to 15 m in width perpendicular to the stream and covered in most cases the full extent of the banks in the direction perpendicular to the stream. An inspection of the LiDAR data (May 2005), Ultracam-D image data (April 2008), and the field data (October 2009) revealed that the condition of the study sites had not changed significantly between the different acquisition dates. This assumption was supported by below average annual rainfalls and a peak flow of 115 ml/day ($1.33\ m^3\ s^{-1}$) between May 2005 and October 2009.[44,45] The bank-full flow level for the Werribee River at Bacchus Marsh was 4.4 m, or 37,167 ml/day ($430\ m^3\ s^{-1}$), and the maximum flow between LiDAR data and optical image acquisition dates had an average recurrence interval of 1.12 years. This period of low flow and channel modification was also confirmed by a comparison of existing ISC field observations and photographs from 2004 and 2008.[47]

The position was measured for all four corners of each plot using two 12-channel Global Positioning System (GPS) receivers and averaging the position for at least one of the corners for more than 1000 s or until the estimated positional error was <2 m. The exact location of the plots was then identified in the field using a field laptop, ArcGIS, and the Ultracam-D image data. A polygon covering the extent of the field plots was manually drawn in ArcGIS at the time of the field survey. An ISC bank condition score was assigned to each of the field plots based on the bank characteristics outlined in Table 2 and Fig. 2.

2.3 *Image Data*

2.3.1 *Multispectral airborne imagery*

Airborne Vexcel Ultracam-D image data were captured on April 19, 20, and 23, 2008, at a spatial resolution of 0.25-m pixels consisting of four multispectral bands located in the blue, green, red, and near infrared parts of the spectrum. The image data were captured at ~3000 m height with side and forward overlaps of 30% and 70%, respectively. A total of 448 frames (7500×11500 pixels per frame) were captured at 16 bits. These data were orthorectified by the data provider and delivered in at-surface radiance values. The Ultracam-D image data were not atmospherically corrected as time series analysis of consecutive image data was not required for this study, and detailed information on the atmospheric conditions at the time of data collection was not available. Based on 10 field–derived ground control points using a 12-channel GPS receiver with the position averaged >1000 s, the root mean squared error (RMSE) was found to be 1.4 m. The custodian of the Ultracam-D image data is the Victorian Department of Sustainability and Environment.

2.3.2 *LiDAR data*

The LiDAR data used in this study were captured using the Optech ALTM3025 sensor between May 7 and 9, 2005, for the study area. The LiDAR data were captured with an average point spacing of 1.6 m ($0.625\ points/m^2$) and a laser footprint size of 0.30 m and consisted of two returns, first and last returns, as well as intensity. The LiDAR returns were classified as ground or nonground by the data provider using proprietary software. The LiDAR data were captured at ~1500 m above ground level. The maximum scan angle was set to 40 deg with a 25% overlap of different flight lines. The estimated vertical and horizontal accuracies were <0.20 and <0.75 m,

Table 1 Field-based measurements and observations related to bank condition.

Measure	Method
Plot dimensions	Tape measure length and width between plot corner markers (m). Measurement accuracy of approximately 0.10 m.
Plot position	Description of position in reach, e.g., meander bend, point bar, straight section, bedrock, and island.
Vegetation ground cover	The areal extent of vegetation ground cover and bare ground (%) was derived by visually estimating the ground cover with 2 m × 2 m within each plot. Vegetation ground cover included green and senescent grass, shrubs, and forbs, whereas litter and bare ground cover were not included. Because of the very dense ground vegetation and understory within parts of the riparian areas, a visual assessment approach was deemed most suitable and logistically possible. A plot size of 4 m^2 was selected as smaller plot sizes can result in larger variation in visual observations (Ref. 48). The average vegetation ground cover within each plot was calculated to the nearest 5%.
Plant projective cover (PPC)	PPC was assessed using a digital camera to obtain upward looking photos taken at 5-m intervals within each plot. These photos were subsequently analyzed to divide the photos into canopy cover and sky using the approach outlined by Johansen et al. (Ref. 46) to estimate PPC.
Surface character	Visual assessment classifying the plot as smooth, hummocky or uneven.
Bank slope	Clinometer measure of average and maximum bank slope (degrees) within the plot area.
Bank-full width	Distance measured from the top of bank to opposite top of bank using a laser range finder with an accuracy of 0.5 m.
Bank height	Bank height was calculated from the field-derived measure of average bank slope and the plot width of the bank section assessed.
Streambed width	Distance measured from the bank toe to opposite bank toe using a laser range finder or tape measure with an accuracy of 0.5 m.
Erosion processes	The method of Hupp et al. (Ref. 49) was used to classify the erosion processes on both sides of the stream (fluvial entrainment was only assessed on the plot side).
Exposed woody roots	Visually estimated into three classes of plot areal coverage (0, <33%, >33%).
Crenulation of banktop	Scalloping of the edge of the bank top was visually assessed as: 0 = none; 1 = small indents in the bank surface of >0.3 m and <1 m from the extrapolated bank edge; 2 = 1 large indent >1 m and small indents; and 3 => 1 large indent >1 m and small indents. The distance along the bank top contour line and the Euclidean distance within each plot were also measured.
Bank type	The homogenous plots were categorized as: vertical/undercut; vertical bank with slumped material at toe; steep >45 deg, but not vertical; gentle <45 deg; composite, complex profile; natural berm, transitional feature; re-sectioned, reprofiled; concave; convex; and planar.
Valley confinement	Valley confinement was noted in the field by labelling the bank: (a) "not confined" if a floodplain wider than 10 m in the direction perpendicular to the stream occurred; (b) "confined" if no floodplain occurred and the landscape kept increasing in height beyond the point of estimated bank-full width; and (c) "partly confined" if one side of the bank was classified as confined and the other as not confined.
ISC 2004 score	The score from the ISC 2004 method was assessed and assigned to each plot using Table 2 (Ref. 10).

Table 2 ISC bank condition scores used in the field assessment (Ref. 10).

ISC bank condition score	Description
4	Very few local bank instabilities, none of which are at the toe of the bank; continuous cover of woody and/or grassy vegetation; gentle batter; very few exposed tree roots of woody vegetation; erosion resistant soils.
3	Some isolated bank instabilities, though generally not at the toe of the bank; cover of woody and/or grass vegetation is nearly continuous; few exposed tree roots of woody vegetation.
2	Some bank instabilities that extend to the toe of the bank (which is generally stable); discontinuous woody and/or grassy vegetation; some exposure of tree roots of woody vegetation.
1	Mostly unstable toe of the bank; little woody and/or grassy vegetation; many exposed tree roots of woody vegetation.
0	Unstable toe of bank; no woody and/or grassy vegetation; very recent bank movement (trees may have recently fallen in stream or obvious bank collapses are present); steep bank surface; numerous exposed tree roots of woody vegetation; erodible soils.

respectively. GPS base stations were used to improve the geometric accuracy of the dataset and validate the vertical and horizontal accuracies. The standard error of ground elevation data compared to 537 field survey points was 0.053 m. The custodians of the LiDAR data are Melbourne Water and the Victorian Department of Sustainability and Environment.

3 Methods

3.1 *Production and Extraction of Image-Based Biophysical Parameters*

In this research, bank condition was defined as the state of the bank at a particular instance in time. The use of remotely sensed imagery will, in the first instance, provide a single-temporal dataset. Multitemporal imagery may allow rates and volumes of material eroded and deposited to be calculated through detection of changes in images.[18,31,36] To provide some information on erosion, i.e., the removal of sediment over time, both the geomorphic characteristics and vegetation cover of the banks were investigated from the remotely sensed dataset. Geomorphic characteristics may provide an indication of historical bank failures. This is usually from large and episodic mass failures that encroach onto the floodplain surface such as rotational or slab failures.[50] Structural vegetation information may indirectly indicate variation since actively eroding sites limit vegetation establishment on the bank face. The combination of limited vegetation cover and steep riverbanks with little downstream variability of the bank top and mean reach width may indicate fluvial entrainment.

The aim was to model the ISC bank condition scores using biophysical parameters derived from remotely sensed data that are likely to explain most of the variability observed in the ISC bank condition scores of the assessed plots. It was not considered to be an issue that the field-based qualitative assessment producing the ISC bank condition scores are not directly compatible with remotely sensed quantitative measurements because of the modeling approach used. The image-based biophysical parameters considered likely to be correlated with field-derived bank condition scores within the study area included: (1) average bank slope; (2) maximum bank slope; (3) plant projective cover (PPC); (4) bank-full width; (5) valley confinement; (6) bank height; (7) bank top crenulations; and (8) percentage vegetation ground cover (Table 3).

3.1.1 *LiDAR-derived digital terrain model*

A digital terrain model (DTM) was produced by inverse distance weighted interpolation of returns classified as ground hits. Several interpolation approaches, including nearest neighbor, inverse distance, and natural neighbor, were assessed and resulted in very similar results.

As inverse distance weighted interpolation is computationally simple and commonly used, this interpolation was applied. The DTM was produced at a pixel size of 1 m.

3.1.2 *LiDAR-derived slope*

From the DTM, a raster surface representing slope, i.e., rate of change in horizontal and vertical directions from the center pixel of a 3×3 moving window and variance of the slope within a moving window of 3×3 pixels, was calculated using ArcMap 9.2. The LiDAR-derived slope layer was used to automatically extract all pixels representing slope within each stream bank plot using ENVI 4.6. Within each field plot, the average and maximum slope values were extracted.

3.1.3 *Mapping fractional and PPC*

Fractional cover count is defined as one minus the gap fraction probability, i.e., the probability of an unobstructed path between the point and range in a set direction.[52] This measure was

Fig. 2 Field photos of different levels of bank condition in relation to the Index of Stream Condition (Ref. 10).

Table 3 Explanatory variables derived from the airborne LiDAR and optical image data and used for comparison with the field-based ISC bank condition scores.

Variable	Image data used for mapping variable	Definition
Bank slope	LiDAR-derived terrain slope	Terrain slope, i.e., change in elevation as a function of the distance between the toe and the top of the stream bank (equal to the plot width).
Plant protective cover	LiDAR-derived cover fraction	Percentage of ground area covered by the vertical projection of vegetation, trunks and branches (Ref. 51).
Streambed width	LiDAR-derived terrain slope and DTM, stream centerline shapefile	The horizontal distance from the toe of the lowest bank to the opposite bank.
Bank-full width	LiDAR-derived terrain slope and DTM, streambed extent	The horizontal distance from the top of the lowest bank to the opposite bank (Ref. 10), often occurring with an obvious break in slope that differentiates the channel from the relatively flat floodplain (Ref. 35).
Valley confinement	LiDAR-derived terrain slope and DTM	System where watercourse is located in a well-defined valley corridor with streams abutting hill slopes of colluvial material (as opposed to alluvial material). Relatively flat areas consisting of alluvial material, extending >10 m beyond the top of the stream bank were classified as unconfined floodplains.
Bank height	LiDAR-derived DTM, streambed extent, bank-full width	The height difference between the toe of the bank (edge of the streambed layer) and the highest point of the first bank also used to define bank-full extent.
Crenulation of banktop	LiDAR-derived contour lines	Crenulation or scalloping of the edge of the bank top was defined as the ratio of the distance along the bank top contour line and the Euclidean distance.
Percentage vegetation ground cover	LiDAR-derived PPC, Ultracam-D image data	Vegetation less than 2 m tall, including both photosynthetically and nonphotosynthetically active vegetation (green and senescent). Vegetation ground cover mainly consisted of grass and shrub within the riparian study area.

calculated from the proportion of counts from LiDAR first returns >2 m above ground level within 5 m × 5 m pixels. The height threshold of 2 m above ground was set to match field measurements of PPC and avoid the inclusion of nonwoody ground cover such as grass. The pixel size was set to maximize the spatial resolution, and at the same time, reduce the number of pixels without data, i.e., areas within each bin without any first and last returns producing null values. PPC, defined as the vertically projected percentage cover of photosynthetic and nonphotosynthetic foliage and branches, was calculated from fractional cover counts using the method presented by Armston et al.[53]

3.1.4 *Mapping bank-full width*

Mapping bank-full width was achieved using object-based image analysis (OBIA) and the eCognition Developer 8 software through a two stage process,[54,55] first including the mapping of streambed extent and then mapping the bank-full width using the LiDAR-derived DTM and slope layers. The OBIA approach used was similar to the one presented by Johansen et al.[56] To map the extent of the streambed, a shapefile representing the stream centerline was used as a basis to grow this line until the steeper stream banks were reached. The classification of the streambed was used to identify the streamside edge of the stream bank. As the bank-full width was mapped in this case, as opposed to the riparian zone extent as reported by Johansen et al.,[56] the last stage in the rule set used for mapping riparian zone extent was omitted,

i.e., no adjustment to riparian zone edges was made based on PPC, to ensure the mapping of bank-full width was based on geomorphic features only.

3.1.5 *Mapping valley confinement*

In some regions of the study area, the river was in direct contact with, or confined by, the hill slope (colluvial) material, often consisting of large boulders or bedrock. Hence, the study area was mapped into confined and unconfined valleys, as the presence of steep unvegetated banks could not be related to bank condition within confined valleys. OBIA was used to map confined and unconfined valleys. In areas with confined valleys, no floodplains were present. Hence, some empirical assumptions were made based on the geomorphic characteristics of the study area and associated terrain slope using the LiDAR-derived slope and DTM layers. The mapped bank-full width was used to provide contextual information for developing a rule set in eCognition Developer 8 for mapping valley confinement. The unclassified areas bordering the stream banks (based on mapped bank-full width) were assessed at the object level. A chessboard segmentation was applied to segment unclassified areas into objects of 5×5 pixels. Those objects bordering the stream banks were classified as floodplains if their slope <7% and their standard deviation of DTM values <0.6, indicating flat areas with limited variation in elevation. Using a region growing algorithm, neighboring objects were classified based on the same criteria until an elevation difference of 5 m above the top of the stream bank elevation was reached. The edge pixels of the stream banks were then classified into unconfined valleys, where the relative area of floodplains within a radius of 15 m of the stream bank edge pixels was above 20%. If this condition was not fulfilled, the stream bank edge pixels were classified as confined valleys. These empirically derived thresholds were based on the definition of confined valleys (Table 3).

3.1.6 *Mapping bank height*

Measurements of bank height were derived at the stream bank plot level using DTM values within each plot for those areas classified as bank-full width. First, the edge pixels of both the streambed and the top of the bank were identified. Then, the mean DTM value of the streambed edge pixels was subtracted from the mean DTM value of the edge pixels of the bank top, providing a measure of bank height.

3.1.7 *Mapping crenulation*

Crenulation or scalloping of the edge of the bank top was used as an indicator of mass failures.[50] It was assessed from the 0.5-m contour lines (lines indicating similar terrain height at 0.5-m intervals) and produced in ArcGIS based on the DTM. To derive a measure of crenulation within each plot, the distance along the contour line and the Euclidean distance from the start and end points of the contour line were measured and divided by each other at the stream bank plot level.

3.1.8 *Mapping percentage vegetation ground cover*

Percentage vegetation ground cover, defined as the percentage cover of the ground by photosynthetically and nonphotosynthetically active vegetation (mainly grass and shrub within the study area) <2-m tall, was mapped from the Ultracam-D and LiDAR data. Along the stream banks, several areas had both green and dry grass. To estimate percentage vegetation cover (including both ground, mid story, and over story cover), the Perpendicular Distance 54 (PD54) index was used.[57] This is a well-established vegetation cover index that has proven successful in areas with multiple types of both dry and green vegetation.[58–60] The PD54 index uses the green and red spectral space to derive an upper limit line for soils (based on selected sites with soil) [Fig. 3(c)] and a lower limit line for pixels representing 100% vegetation cover [Fig. 3(d)]. Observations between the soil and 100% vegetation cover lines suggest a mixture of soil and vegetation. The perpendicular distance from the soil line in green-red spectral space then becomes the percentage vegetation cover, scaled based on the distance between the soil and

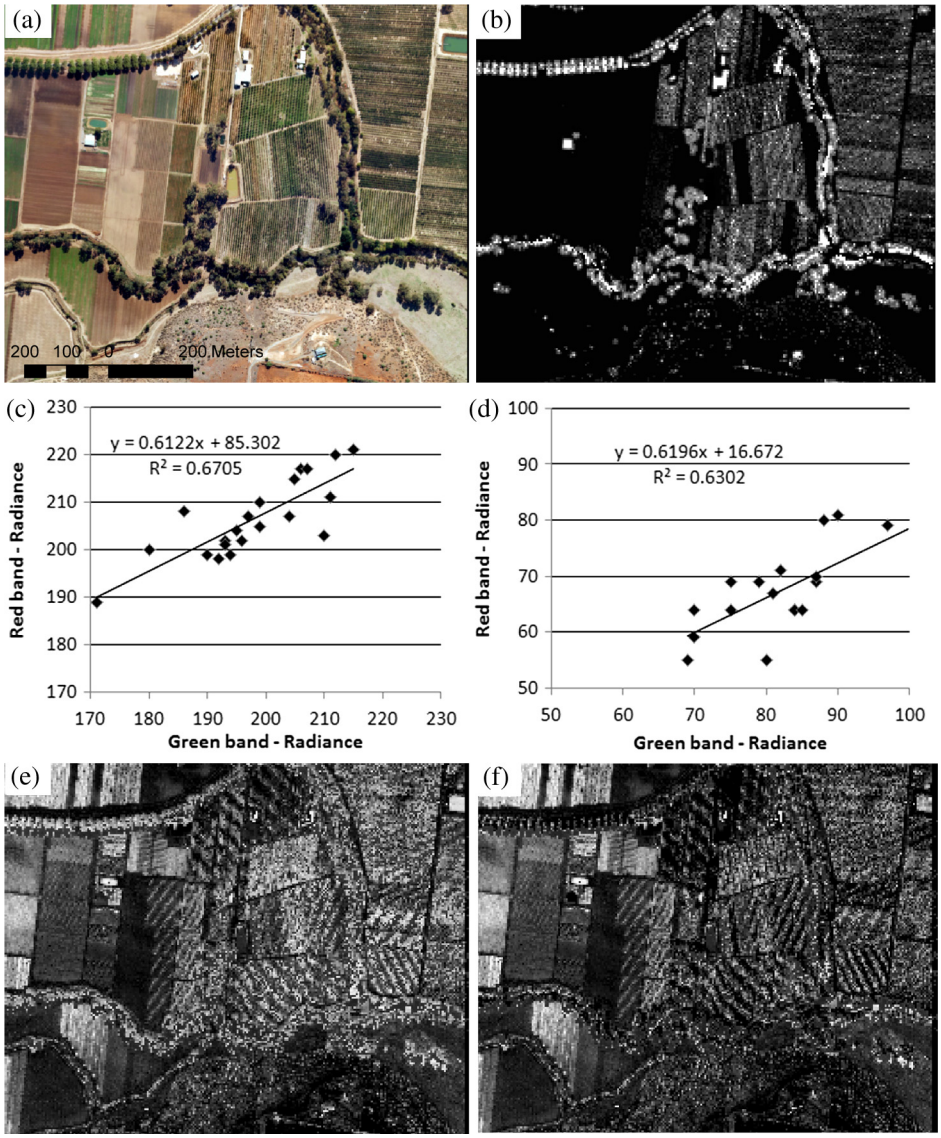

Fig. 3 Workflow for production of percentage vegetation ground cover using the Ultracam-D and LiDAR data: (a) Ultracam-D imagery; (b) LiDAR-derived PPC; (c) soil line based on Ultracam-D imagery; (d) vegetation line based on Ultracam-D imagery; (e) percentage vegetation cover using the PD54 index; and (f) percentage vegetation ground cover produced by combining the Ultracam-D derived PD54 index and the LiDAR-derived PPC layers.

100% vegetation cover lines [Fig. 3(e)].[57] Sites visited in the field were used to select soil samples within the streambed to produce the soil line, whereas sites with 100% vegetation ground cover were selected to produce the 100% vegetation cover line. To ensure pure soil and vegetation pixels were used, the Ultracam-D image data with 0.25-m pixels were used. Only sites with 100% vegetation ground cover and no canopy cover were selected to establish the vegetation line because the vegetation ground cover tended to have slightly higher radiance values than dense canopy cover. Based on the soil and vegetation lines, the percentage vegetation cover was calculated for the Ultracam-D image after the pixel size had been resampled to 5 m to match with the pixel size of the LiDAR-derived PPC layer. While the selection of dense vegetation ground cover sites improved the scaling of percentage vegetation ground cover using the PD54 index, it resulted in very dense canopy cover being mapped with >100% vegetation cover because of the canopy cover appearing darker than vegetation ground cover in the green-red spectral space

due to the in-crown shadowing effects. Hence, these values were subsequently set to 100%. This was not considered an issue as the LiDAR data were used to remove overstory cover to estimate percentage vegetation ground cover [Fig. 3(f)]. Based on the results of this research and the fact that many riparian zones in Australia have limited or no vegetation ground cover underneath areas with very dense overstory canopy cover, the removal of the PPC component from the PD54 cover estimate was considered important. The estimation of percentage vegetation ground cover, i.e., vegetation of < 2 m height, was accomplished using the LiDAR-derived estimates of PPC and Eq. (1):

$$\%\text{vegetation\_groundcover} = \frac{(\text{PD54cover} - \text{PPC}_{\text{LiDAR}})}{(1 - \text{PPC}_{\text{LiDAR}})}. \quad (1)$$

Because of the careful selection of pixels representing the soil and 100% vegetation cover line, there were only very few occurrences where $\text{PPC}_{\text{LiDAR}} > \text{PD54 cover}$. In those cases, where $\text{PPC}_{\text{LiDAR}} > \text{PD54 cover}$, the resulting negative values were set to 0%.

3.2 *Validation of Image-Based Biophysical Parameters*

Modeling bank condition based on image-derived biophysical parameters relies on their accurate mapping. Hence, the accuracy of the image-based biophysical parameters was assessed. The accuracy assessments were carried out by comparing field measurements with the corresponding image-derived biophysical parameter measurements. With the exception of valley confinement, linear regression based on produced scatterplots between the field- and image-based measurements was used for validation to assess the model fit.

- Bank slope measurements derived in the field for each plot were related to the LiDAR-derived slope layer using the mean of all the pixels occurring within each plot as the field-derived slope measurements were considered representative at the plot level.
- A total of 242 upward looking photos were taken in the field and converted to a measure of PPC (Table 1). However, to minimize effects of any horizontal offsets between the field photos and the LiDAR data, the accuracy of LiDAR-derived PPC was assessed at the object level against the average of the PPC field measurements occurring within each object.[46] This produced 68 samples.
- The streambed and bank-full widths measured in the field were compared to the widths mapped from the OBIA at the corresponding location.
- The validation on mapped valley confinement was carried out by using the 50 locations visited in the field, where valley confinement was noted on each bank side, producing a total of 100 observations. User's and producer's accuracies were calculated.
- In eCognition Developer 8, the edge pixels bordering the streambed (toe of the bank) and unclassified parts of the image (top of the bank) were classified within each of the field plots. The average DTM elevation of the edge pixels representing the toe of the bank was subtracted from the average DTM elevation of the edge pixels representing the top of the bank. This produced a measure of bank height for each plot, which was compared to the corresponding field-derived bank height measurements.
- Crenulation, i.e., the ratio of the distance along the bank top contour line and the Euclidean distance, assessed in the field was compared to the corresponding measurements derived from the DTM contour lines closest to the top of the bank.
- Field estimates of percentage vegetation ground cover within each field plot were compared to the image-derived average of percentage vegetation ground cover of the pixels within each field plot.

3.3 *Predictive Modeling*

Initially, a number of linear scatter plots were produced to assess the relationship between the ISC bank condition scores of the field plots and the image-derived variables of the corresponding

locations in the image data. Those biophysical parameters that produced a clear relationship with the field-based ISC bank condition scores were selected for the modeling using either linear or logarithmic relationships. An interaction term, i.e., multiplication of two explanatory variables, in this case, percentage vegetation ground cover and average bank slope, was also produced to add additional information to the model. When considered individually, it was found reasonable to expect that an increase in vegetation ground cover would lead to an increase in bank condition scores and that an increase in slope would lead to a decrease in scores. The effects of vegetation ground cover might be diminished at low slopes or be even negligible. However, vegetation ground cover at high slopes might have a significant effect. Hence, this interaction term was considered important based on a reasonable physical relationship. The modeling procedure was implemented in the statistical analysis software package R version 2.10.1,[61] using the combination of variables deemed most suitable from the univariate regression analysis.

The relationship developed between the field assessed ISC bank condition scores consisted of five values on an ordinal scale and image-derived parameters consisted of continuous data values, so a cumulative logistic regression model for multinomial response variables was found appropriate.[62] Other statistical approaches, including partial proportional odds models (constrained and unconstrained) and machine learning approaches (support vector ordinal regression and neutral network ordinal regression), were considered. However, these methods can be very difficult and time consuming to apply or interpret and are unlikely to yield much improvement on a small dataset.

Those valley confined sections visited in the field occurred either in gorge or upland sections. The reference for a confined valley section is guided by the fact that the river is in contact with hill slope (colluvial) material rather than stream bank (alluvial) material. Often, the bank material in confined sections is large (boulders) or bedrock. The presence of steep-unvegetated banks is therefore an inappropriate reference for these bank types and it was decided to leave these out and classify areas with confined valleys separately. The predictive models had the following form:

$$p_n = \beta_0 + \beta_1 \text{Metric1} + \beta_2 \text{Metric2} + B_{n-1} \text{Metric}(n-1) + \beta_n \text{Metric}(n) \tag{2}$$

and

$$p(\text{ISCscore\_}n) = \frac{e^{pn}}{1 + e^{pn}}. \tag{3}$$

In this case, four β_0 intercept values were produced, representing the cumulative probability for deriving an ISC score of: 0; 0 and 1; 0, 1, and 2; and 0, 1, 2, and 3. The probability of deriving an ISC score of 4 then becomes 1 minus the probability of deriving the cumulative ISC bank condition score of 0, 1, 2, and 3. In addition, $\beta_1, \beta_2 \ldots \beta_{n-1}, \beta_n$ values were derived for the biophysical parameters included in the model.

3.4 *Comparison of Predicted and Observed ISC Scores*

To compare the model outcome with the ISC scores, a confusion matrix and related overall accuracy were produced in the statistical software package R. A graph showing observed versus predicted ISC bank condition scores was also produced. Since these comparison measures include the data used to train the model, the estimates are likely to be optimistic. A 10-fold cross-validation of RMSE was used to provide a more realistic estimate of the predictive accuracy of the model. The overall accuracy was also calculated including the plots located in areas with confined valleys. To produce a realistic measure of misclassification error, cross-validation was used in 10 loops, where 10% of the data were left out each time for validation.

Probability plots for each bank condition category of the cumulative logistic regression models were produced to assess the model sensitivity of the reported RMSE for each of the variables included in the predictive modeling of bank condition. These plots were produced for the individual explanatory variables with the assumption that the remaining explanatory variables were

kept constant at the average value extracted from the image data set for the plots visited in the field.

4 Results

This section first presents the mapping accuracies of the LiDAR and Ultracam-D derived layers assessed in this research. Then, the results of relating the field assessed bank condition scores and remotely sensed biophysical parameters are shown. Finally, the predictive models and an applied mapping result are presented.

4.1 *Image-Based Biophysical Parameters*

The maps of the biophysical parameters and thematic information used to predict the ISC bank condition scores are presented in Fig. 4. The associated mapping accuracies and model fits of the LiDAR and image-derived variables are presented in Fig. 5. The model fit of the individual biophysical variables was all statistically significant ($P < 0.001$), with R^2 varying between 0.75 and 0.95. Out of the 100 field-based observations of confined and unconfined valleys, only one location with an unconfined floodplain was classified as valley confined because some local variability in the terrain elevation near the bank top did not fulfill the conditions in the rule set of the OBIA.

4.2 *Relation of Biophysical Parameters to Bank Condition*

Box and whisker plots relating field assessed ISC bank condition scores and the image-derived biophysical parameters were produced to identify those image biophysical parameters that were most suitable to include in the predictive modeling (Fig. 6). Those biophysical parameters showing the highest correlation with ISC bank condition scores were average terrain slope ($R^2 = 0.60$, $n = 41$, $P < 0.001$) and maximum terrain slope ($R^2 = 0.58$, $n = 41$, $P < 0.001$) within the field plots, with increasing terrain slope producing lower bank condition scores. However, average terrain slope within plots was found more reliable to use than maximum terrain slope as the maximum terrain slope value was derived from only one pixel per plot and is hence potentially risky to include as this value is not representative of the plot. The percentage vegetation ground cover within the field plots exhibited a statistically significant positive relationship with the ISC bank condition scores ($R^2 = 0.43$, $n = 41$, $P < 0.001$). The ratio of bank-full width and bank height also showed statistically significant positive relationships with ISC bank condition scores ($R^2 = 0.31$, $n = 41$, $P < 0.001$). Using the logarithm of the ratio of bank-full width and bank height increased the R^2 to 0.41. This suggests that narrow streams with high banks have lower bank condition scores than wider streams with low banks within the study area.

The relationship between bank top crenulation and ISC bank condition scores was negative and statistically insignificant. There was insufficient evidence to support the hypothesis that scalloped banks were associated with lower bank condition scores. No statistically significant correlations between field-assessed ISC bank condition scores and PPC were observed. As a consequence, bank top crenulation and PPC were excluded from the predictive models.

4.3 *Predictive Models*

Cumulative logistic regression models were developed for calculating the probability of a given value of average slope, bank-full width/height ratio, percentage vegetation ground cover, and an interaction term (percentage vegetation ground cover multiplied with average slope) belonging to a bank condition score of 0, 1, 2, 3, or 4 within the corresponding plots. The results of the model building are shown below [Eqs. (4)–(7)]. The model that produces the highest probability value will indicate the most likely bank condition score for the plot under consideration. An example of applying the predictive models [Eqs. (4)–(7)] is provided in Fig. 7 for a section without valley confinement.

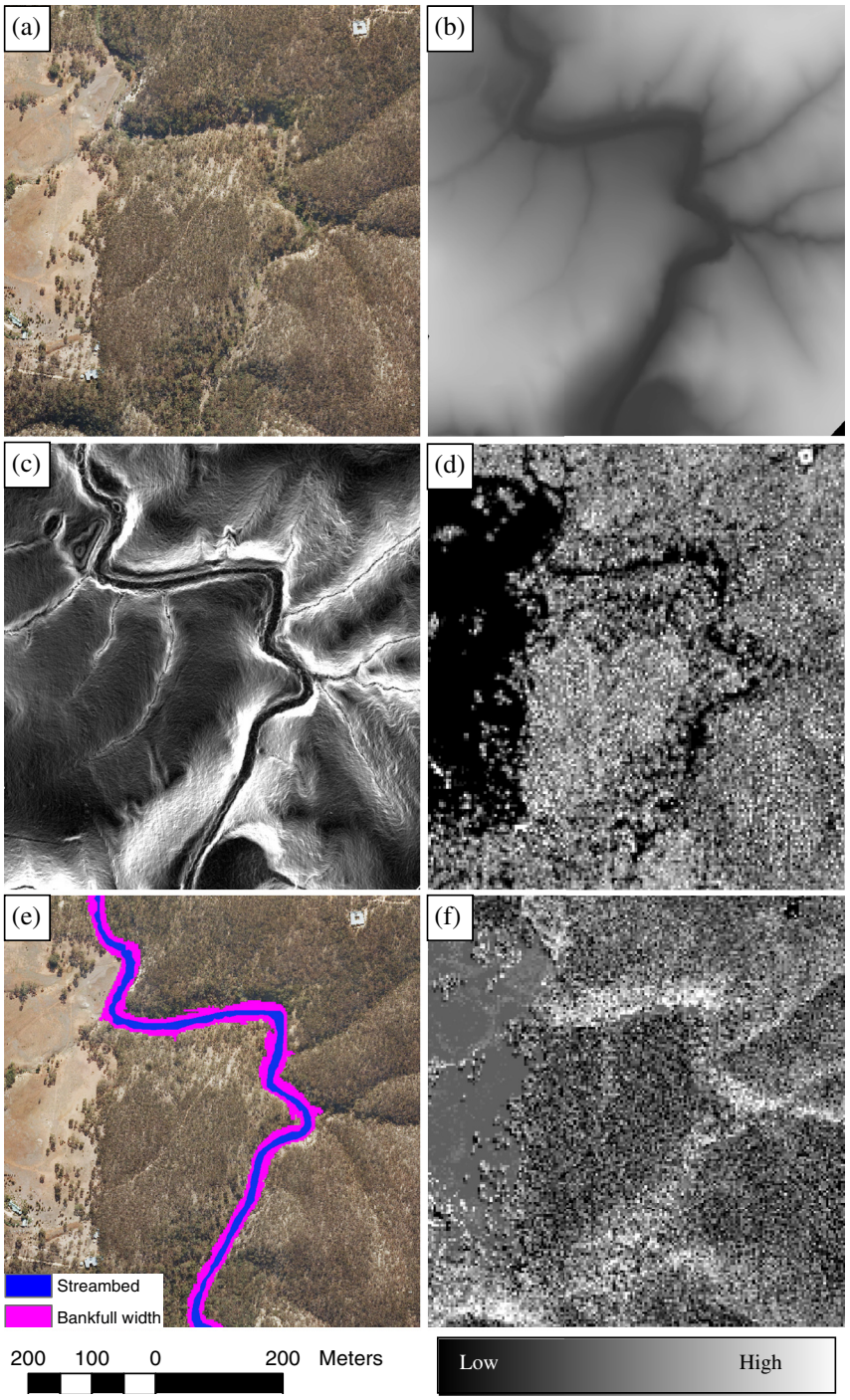

Fig. 4 Input layers of biophysical parameters and thematic information used for predicting ISC bank condition scores: (a) true color Ultracam-D image; (b) DTM; (c) terrain slope; (d) PPC; (e) streambed and bank-full widths; and (f) vegetation ground cover.

$$p(\mathrm{ISCscore0}) = \frac{e^{-5.5057+\left[-2.5551\times\ln\left(\frac{\mathrm{Bankwidth}}{\mathrm{Bankheight}}\right)\right]+3.4191\times\%\mathrm{grasscover}+0.4665*\mathrm{AveSlope}+[-0.4224\times(\%\mathrm{grasscover}\times\mathrm{AveSlope})]}}{1+e^{-5.5057+\left[-2.5551\times\ln\left(\frac{\mathrm{Bankwidth}}{\mathrm{Bankheight}}\right)\right]+3.4191\times\%\mathrm{grasscover}+0.4665\times\mathrm{AveSlope}+[-0.4224\times(\%\mathrm{grasscover}\times\mathrm{AveSlope})]}}, \quad (4)$$

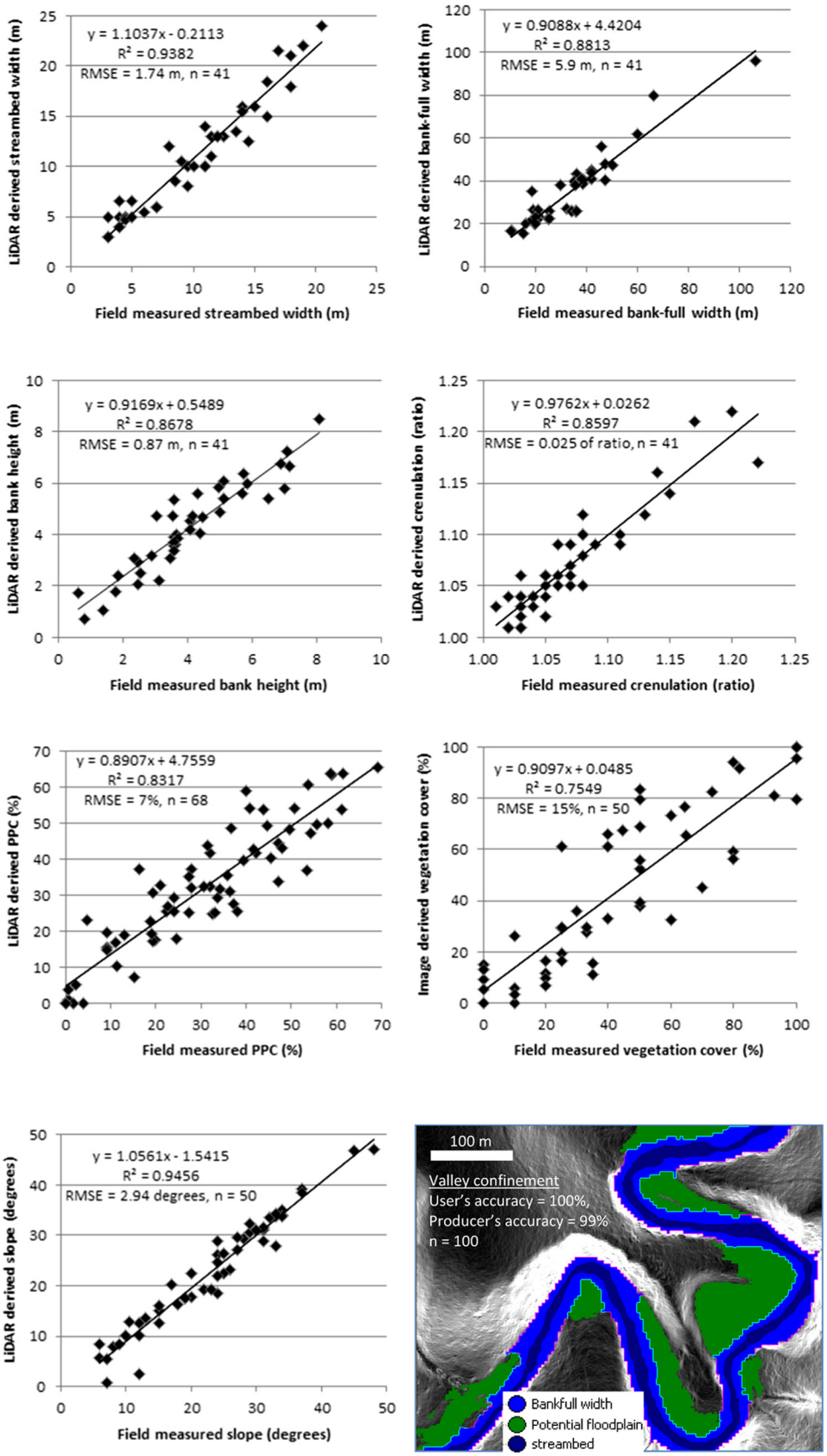

Fig. 5 Scatterplots and accuracy measures of LiDAR and optical image-derived bank form and vegetation biophysical variables, as well as valley confinement, mapped and used for modeling ISC bank condition scores.

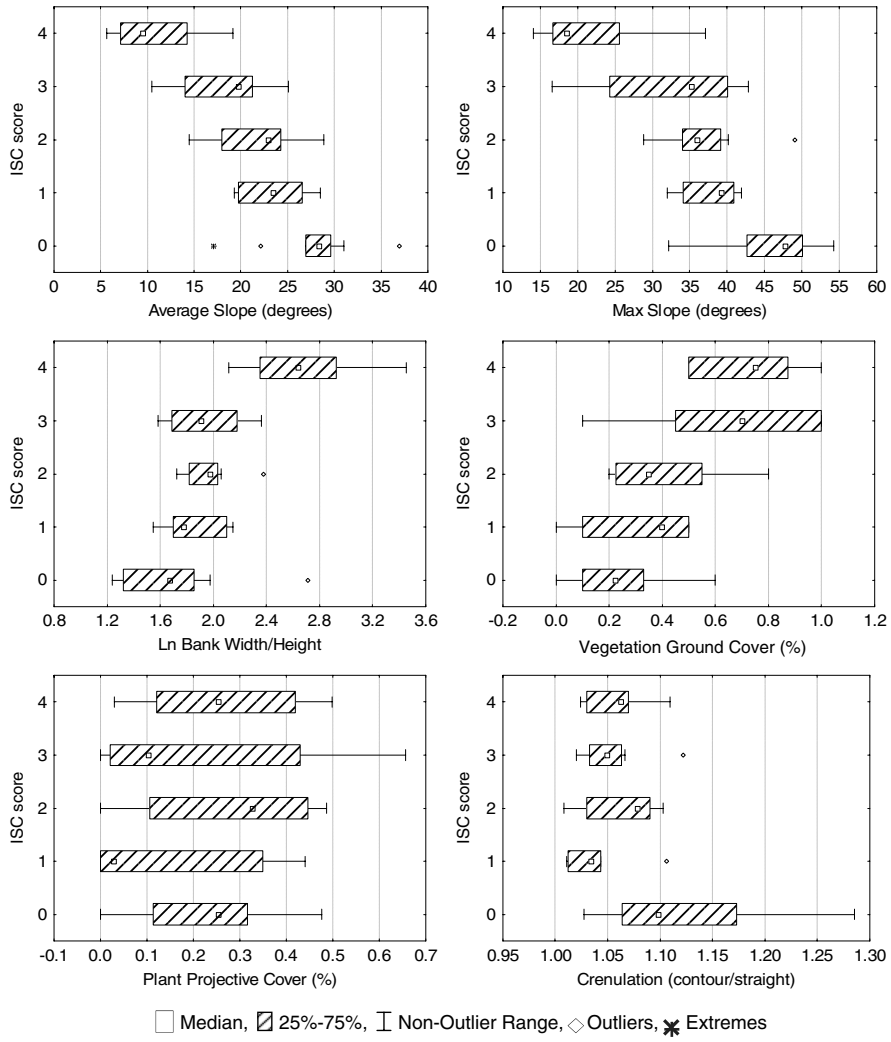

Fig. 6 Box and whisker plots showing the median, 25% and 75% percentiles (box), 1 and 99 nonoutlier range (whiskers), outliers and extreme values of average slope, maximum slope, the logarithm of bank width/height ratio, vegetation ground cover, PPC, and crenulation in relation to individual ISC bank condition scores.

$$p(\text{ISCscore0, 1}) = \frac{e^{-3.7139+\left[-2.5551\times\ln\left(\frac{\text{Bankwidth}}{\text{Bankheight}}\right)\right]+3.4191\times\%\text{grasscover}+0.4665\times\text{AveSlope}+[-0.4224\times(\%\text{grasscover}\times\text{AveSlope})]}}{1+e^{-3.7139+\left[-2.5551\times\ln\left(\frac{\text{Bankwidth}}{\text{Bankheight}}\right)\right]+3.4191\times\%\text{grasscover}+0.4665\times\text{AveSlope}+[-0.4224\times(\%\text{grasscover}\times\text{AveSlope})]}}, \quad (5)$$

$$p(\text{ISCscore0, 1, 2}) = \frac{e^{-1.3024+\left[-2.5551\times\ln\left(\frac{\text{Bankwidth}}{\text{Bankheight}}\right)\right]+3.4191\times\%\text{grasscover}+0.4665\times\text{AveSlope}+[-0.4224\times(\%\text{grasscover}\times\text{AveSlope})]}}{1+e^{-1.3024+\left[-2.5551\times\ln\left(\frac{\text{Bankwidth}}{\text{Bankheight}}\right)\right]+3.4191\times\%\text{grasscover}+0.4665\times\text{AveSlope}+[-0.4224\times(\%\text{grasscover}\times\text{AveSlope})]}}, \quad (6)$$

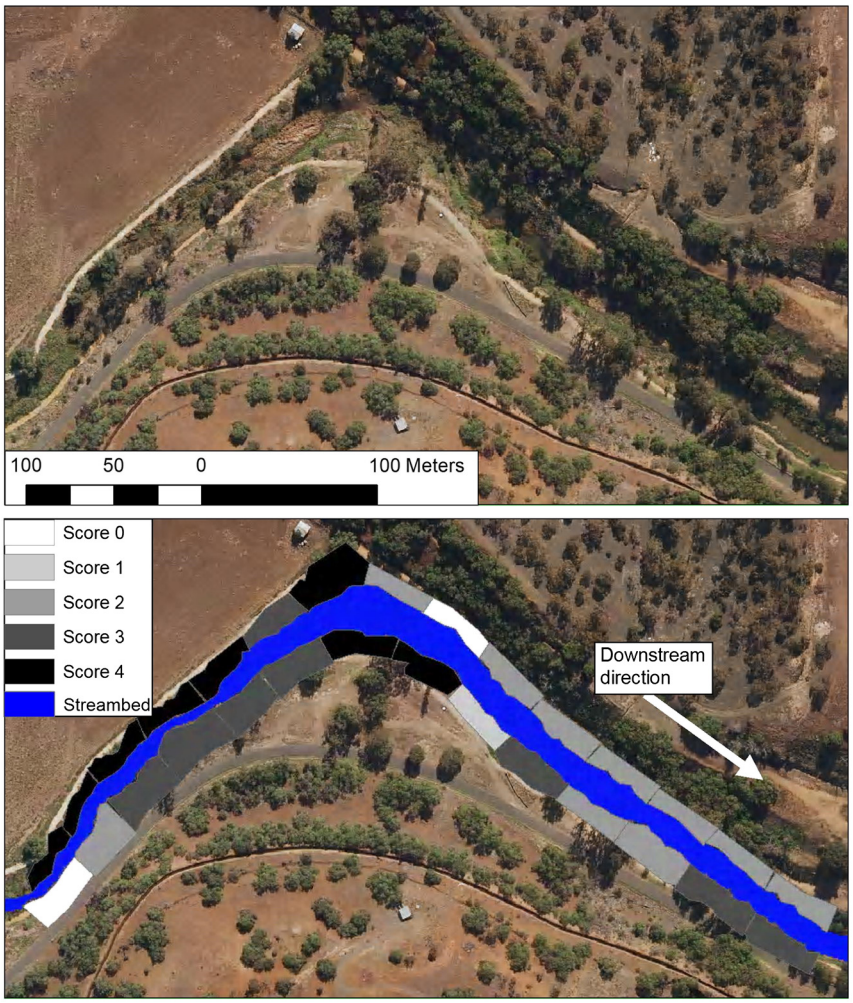

Fig. 7 Bank condition scores calculated using the predictive models for manually delineated 50-m long sections for a subset of the Werribee River, Victoria, Australia.

$$p(\text{ISCscore0, 1, 2, 3}) = \frac{e^{1.4418+\left[-2.5551\times\ln\left(\frac{\text{Bankwidth}}{\text{Bankheight}}\right)\right]+3.4191\times\%\text{grasscover}+0.4665\times\text{AveSlope}+[-0.4224\times(\%\text{grasscover}*\text{AveSlope})]}}{1+e^{1.4418+\left[-2.5551\times\ln\left(\frac{\text{Bankwidth}}{\text{Bankheight}}\right)\right]+3.4191\times\%\text{grasscover}+0.4665\times\text{AveSlope}+[-0.4224\times(\%\text{grasscover}\times\text{AveSlope})]}}. \quad (7)$$

4.4 *Comparison of Observed and Predicted ISC scores*

A confusion matrix was produced to compare the observed ISC bank condition scores assessed in the field and the predicted values. The confusion matrix was produced for 41 observations, excluding the plots with confined valleys (Table 4 and Fig. 8). Based on the confusion matrix, the overall accuracy was 61%. ISC bank condition scores of 0 and 4 were most accurately predicted. In 13 out of 16 cases where the observed and predicted scores did not match, there was only a difference of one score between them.

The nine plots that were located within a confined valley were all correctly identified using the mapping approach developed in eCognition Developer 8. This increased the overall accuracy to 68%. It should also be noted that the confusion matrix only presents the empirical modeling

Table 4 Confusion matrix comparing the observed and predicted ISC bank condition scores.

ISC score	0 (observed)	1 (observed)	2 (observed)	3 (observed)	4 (observed)	User's accuracy
0 (predicted)	9	2	0	0	0	81.82
1 (predicted)	0	2	3	0	0	40.00
2 (predicted)	1	1	3	2	0	50.00
3 (predicted)	1	1	2	4	1	44.44
4 (predicted)	0	0	0	2	7	77.78
Producer's accuracy	81.82	33.33	37.50	50.00	87.50	

results and not a true comparison because the observed values were used to predict the scores. To obtain a reliable comparison measure, cross-validation was used. A 10-fold cross-validation estimate of the mis-classification RMSE was 0.95 of the ISC bank condition score. This measure indicates that the predictive modeling produced an ISC bank condition score within less than one observed score. The misclassification error of 0.95 was only based on the 41 plots, excluding the plots with valley confinement. As the valley confinement could be reliably mapped, the misclassification error is in reality smaller than 0.95 of the ISC bank condition score. The results of the probability plots of the cumulative logistic regression model showed that the RMSE values derived in the comparison process (Fig. 5) were sufficiently low and did not affect the predicted ISC bank condition score unless the value of the explanatory variable was close to the threshold separating two ISC bank condition scores.

5 Discussion

5.1 *Using Landform and Biophysical Variables to Predict ISC Scores*

Our approach for mapping bank condition from airborne LiDAR and high-spatial resolution image data effectively predicted bank condition based on a subset of image-derived variables. The adoption of image-based biophysical variables that exhibited statistically significant covariation with visual ISC bank condition scores approximated the way humans perceive bank condition. Despite the promising results, it is important to carefully evaluate the spatial scale of applying the approach and how representative the explanatory variables are for the area they are applied to. Therefore, different models may be required for different catchments. For example, previous research established statistically significant correlation between PPC and bank condition in a north Australian woodland riparian environment due to the stabilizing effect of tree roots.[23] While tree canopy cover has been used to guide large spatial scale erodibility modeling,[63] and may be indirectly related to bank strength,[64] the absence of trees does not necessarily mean erosion is occurring. In this study, we obtained field measurements from a range of sites with varying severities of different active bank and fluvial processes. The restriction of data used to train the models from a specific region with a limited range of processes and severity remains. The general applicability of models may increase if more information is used to train the model over a larger area. An alternative would be to create a regionalization of different process dominances,[65] or river type,[3] and create different models with different representative biophysical parameters for each region or type of process.

The outliers of the observed versus predicted bank condition data may provide information on areas where a generic scoring method is inappropriate. Three sites were evident with large differences between predicted and observed ISC scores. In the first example where the observed ISC bank condition score was 0 and the predicted score was 3, the average bank slope was 17 deg, the vegetation ground cover was 60%, and the bank-full width/height ratio was 7.2. These values would, in most cases, have produced ISC bank condition scores of at least 2, but because of two mass failures within the plot, the score was assessed as 0 in the field.

Some crenulation within the plot was observed in the contour lines (ratio of 1.12 between contour line and Euclidean distance). Another outlier with an observed score of 1 and a predicted value of 3 had an average bank slope of 19.7 deg, vegetation ground cover of 50%, and a bank width/height ratio of 8.6. The probability of obtaining a bank condition score of 2 and 3 was 41.1% and 44.6%, respectively. Because of the similar probabilities of deriving a score of 2 and 3, a reduction in the input vegetation ground cover value of 2% would have resulted in a predicted score of 2. The third outlier deviating by more than one score had a field assessed score of 0, but the highest probability score indicated a bank condition score of 2 based on an average bank slope of 22.1 deg, vegetation ground cover of 0%, and a bank width/height ratio of 15. In this case, the relatively high bank-full width/height ratio caused by the limited bank height of 2.54 m and the relatively low average bank slope produced the highest predicted probability for a score of 2. This plot was only 2.5-m wide because of a narrow bank section between the toe and the top of the bank. The bank was vertical in parts and also undercut in some areas.

The limited ability of the LiDAR data to accurately map steep slopes, e.g., >70 deg, should be considered in relation to the narrow bank section and the LiDAR point density of 0.625 points/m^2. Other studies have found that LiDAR point density and DEM resolution have a significant impact on surface slope and surface derivatives.[29,32,66] A LiDAR dataset with a higher point density to increase the number of canopy and ground returns and a derived slope layer with a smaller pixel size would be more suitable for identification of narrow sections with steep bank slopes. If the slope had been increased from 22.1% to 26% while keeping all other explanatory variables constant, the predicted bank score would have been 0.

5.2 *Spatial Scaling Considerations*

It is essential to assess the mapping accuracy of the input layers used for the predictive modeling as the accuracy of these layers may significantly affect the bank condition mapping results. Also, the larger the plots are for assessment of bank condition, the more averaging of bank condition will occur. Therefore, small bank instabilities or erosive features may not be identified for plot sections of ≥ 50 m. Based on the observations in the field, some river and creek stretches showed large variation over short distances (10 to 15 m). It would therefore be important to determine the optimal plot section length to avoid excessive averaging of bank condition. For rivers and creeks in the study area, a plot section length of 10 m would be suitable in most cases based on ISC bank condition score variability and the observed spatial variation in the explanatory variables derived from the LiDAR and optical image data. Therefore, it is also important that the remotely sensed image data have a spatial resolution suitable for detecting bank condition variability. The point density of the LiDAR data used in this research was 0.625 points/m^2. A LiDAR point density of 10 points/m^2 or more would significantly improve the ability to accurately map PPC and vegetation ground cover and detect detailed slope variation of stream banks at higher spatial resolution and enable a reduction of the plot section length.[32,67,68]

For assessment of the mapping results and for comparison of different stream sections, it is recommended that sections covering at least one meander wavelength be used, as the outside of meander bends are often exposed to erosive processes and hence appear with low bank condition scores, whereas point bars are generally more stable.[40] Using at least one meander wavelength for assessment of bank condition mapping results will ensure a less biased comparison of different stream sections. To automate the mapping approach, a method for developing plot sections of equal size is required. These sections should have a set length, e.g., 10 m and a width perpendicular to the stream equal to the bank width on each side of the streams. Once these plots have been automatically produced, the explanatory variables used in the predictive models can be automatically derived and subsequently subjected to the predictive models at the plot level. Future work will focus on automating the mapping process in eCognition Developer 8.

Rehabilitation or restoration in river systems is often undertaken at a reach scale and very infrequently assessed on its subsequent performance.[69] Landholders often apply pressure to government to fix bank erosion as it is a clearly visible process that encroaches onto their property. Accurate spatial information on bank condition, at a catchment scale, allows a more targeted

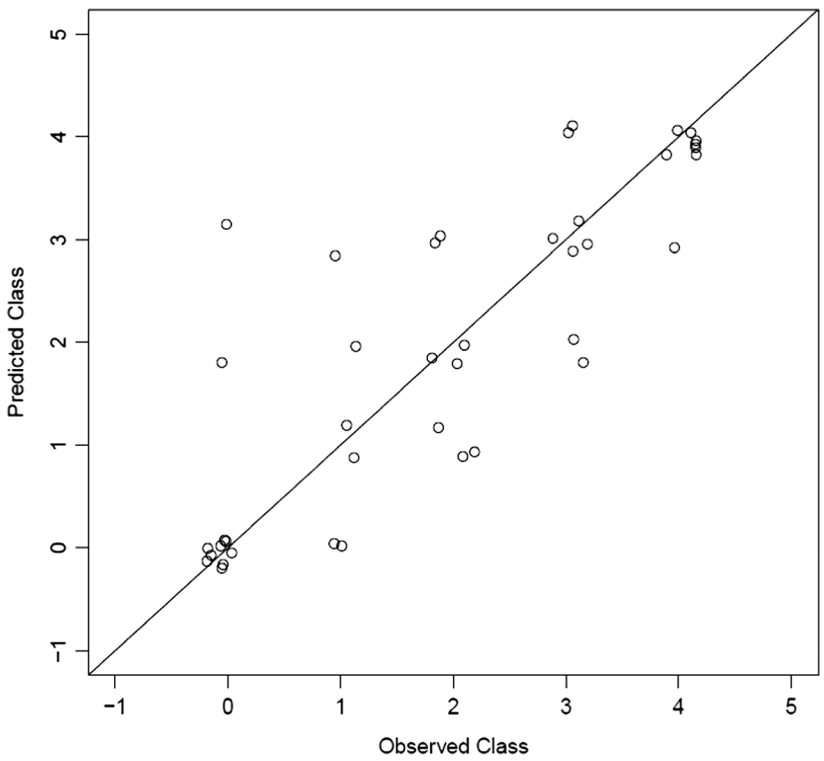

Fig. 8 Plot showing the relationship between the observed and predicted ISC bank condition scores, excluding the nine plots with confined valleys. Also note that points have been jittered for clarity.

approach to management and potential establishment of regulations and other policy mechanisms concerning the environmental condition of streams.

5.3 *Application Value of the Results*

The developed mapping approach provides an opportunity to adopt more rigorous and quantitative approaches to quantify spatial variability of stream bank condition and potentially rates of change in bank condition over time. Although the objective of this research was to assess the capability to use airborne LiDAR and high-spatial resolution optical image data for mapping bank condition using the same scoring system as the ISC field-based approach, it should be highlighted that the remotely sensed method developed represents a quantitative mapping approach compared to the qualitative scoring–based ISC approach. Hence, the differences reported in the comparison of the predicted and observed ISC scores may, to some extent, reflect the difference in scoring-based qualitative techniques and quantitative-based mapping approaches. As shown in Fig. 5, the LiDAR- and image-based mapping accuracies demonstrate the ability to quantitatively measure a large number of variables related to stream bank condition over large spatial extents and with complete spatial coverage, which may in fact be a more significant finding in itself for fluvial geomorphologists and environmental managers than the ability to estimate ISC scores from these remotely sensed quantitative variables. This should especially be considered in relation to the repeatability and consistency of deriving the remotely sensed quantitative measures, whereas assessment bias and interoperator variability of field-based qualitative assessments may reduce the ability to compare different sites or the same site over time in an accurate manner.[15] Hence, the ability of producing accurate measures of bank form and riparian zone biophysical parameters from LiDAR data and high-spatial resolution image data represents an opportunity to move beyond field-based qualitative measures of bank condition toward more direct quantitative and consistent assessment methods of stream bank condition.

6 Conclusions and Future Work

This research presents a method suitable for mapping bank condition based on LiDAR and high-spatial resolution remotely sensed image and field data. The study was undertaken within an area restricted by available imagery. It is possible that adjustments and additional explanatory variables are needed for other areas and streams with different active processes and vegetation and terrain characteristics. A number of different landform and biophysical parameters and characteristics were assessed at the plot level in the field. From the LiDAR and high-spatial resolution image data, the following layers were required for developing the predictive models: (1) DTM, (2) terrain slope, (3) PPC, (4) streambed extent, (5) bank-full width, (6) vegetation ground cover, and (7) contour lines. From these layers, the following explanatory variables could be extracted for comparison against field assessed ISC bank condition scores to produce the predictive models:

- Average bank slope,
- PPC,
- Bank-full width,
- Valley confinement,
- Bank height,
- Crenulation of banks,
- Percentage vegetation ground cover, and
- Bank width/bank height ratio.

Cumulative logistic regression models for multinomial response variables were used for predicting bank condition by calculating the probability of the ISC bank condition scores based on the most suitable explanatory variables. The average bank slope, percentage vegetation ground cover, the bank-full width/height ratio, and an interaction term between average terrain slope and vegetation ground cover were found most suitable for the development of the predictive models. On average, the predicted ISC bank condition scores were within less than one score of the observed ISC bank condition and had an overall accuracy of 68% when including field plots with confined valleys. The developed approach for mapping bank condition may reduce the time and cost of traditional field-based approaches when applied at the reach and catchment scales, which may facilitate future management decision making. In addition, the results highlight the ability to move from field-based qualitative approaches toward more direct unbiased, repeatable, quantitative, and spatially extensive remotely sensed assessment methods of stream bank condition with complete spatial coverage. The approach will be applied to airborne LiDAR and high-spatial resolution optical image data covering 26,000 km of stream length in Victoria, Australia.

Acknowledgments

Paul Wilson, Sam Marwood, and John White from the Department of Sustainability and Environment, Victoria, provided the LiDAR and Ultracam-D image data as well as significant help with fieldwork, image processing, and interpretation of results.

References

1. R. Carballo et al., "WFD indicators and definition of the ecological status of rivers," *Water Resour. Manag.* **23**(11), 2231–2247 (2009), http://dx.doi.org/10.1007/s11269-008-9379-9.
2. A. R. Ladson et al., "Development and testing of an Index of Stream Condition for waterway management in Australia," *Freshwater Biol.* **41**(2), 453–468 (1999), http://dx.doi.org/10.1046/j.1365-2427.1999.00442.x.
3. G. J. Brierley et al., "Application of the River Styles framework to river management programs in New South Wales, Australia," *Appl. Geogr.* **22**(1), 91–122 (2002), http://dx.doi.org/10.1016/S0143-6228(01)00016-9.

4. NRM South (Natural Resource Management South), *Tasmanian River Condition Index, Physical Form Field Manual*, NRM South, Hobart, Tasmania (2009).
5. L. B. Leopold, M. G. Wolman, and J. P. Miller, *Fluvial Processes in Geomorphology*, WH Freeman and Company, San Francisco (1964).
6. A. Laubel et al., "Hydromorphological and biological factors influencing sediment and phosphorus loss via bank erosion in small lowland rural streams in Denmark," *Hydrol. Process.* **17**, 3443–3463 (2003), http://dx.doi.org/10.1002/(ISSN)1099-1085.
7. D. L. Rosgen, *Applied River Morphology*, Wildland Hydrology Books, Pagosa Springs, Colorado (1996).
8. Environmental Agency, *River Habitat Survey: 1997 Field Survey Guidance Manual, Incorporating SERCON*, Environment Agency, Bristol, UK (1997).
9. S. J. Bennett and A. Simon, *Riparian Vegetation and Fluvial Geomorphology*, American Geophysical Union, Washington, DC (2004).
10. ISC, *Index of Stream Condition Users Manual*, 3rd ed., The State of Victoria Department of Sustainability and Environment, Melbourne, Victoria (2006).
11. A. Jansen et al., *Rapid Appraisal of Riparian Condition, Version 2*, River and Riparian Land Management Technical Guidelines No. 4A, Land and Water Australia, Canberra, Australia (2005).
12. G. Werren and A. Arthington, "The assessment of riparian vegetation as an indicator of stream condition, with particular emphasis on the rapid assessment of flow-related impacts," in *Landscape Health of Queensland*, A. Shapcott, J. Playford, and A. J. Franks, Eds., pp. 194–222, The Royal Society of Queensland, St. Lucia, Australia (2002).
13. S. E. Darby and C. R. Thorne, "Development and testing of riverbank-stability analysis," *J. Hydraul. Eng.* **122**(8), 443–454 (1996), http://dx.doi.org/10.1061/(ASCE)0733-9429(1996)122:8(443).
14. A. R. Ladson et al., "Effect of sampling density on the measurement of stream condition indicators in two lowland Australian streams," *River Res. Appl.* **22**(8), 853–869 (2006), http://dx.doi.org/10.1002/(ISSN)1535-1467.
15. K. Johansen et al., "Comparison of image and rapid field assessments of riparian zone condition in Australian tropical savannas," *Forest Ecol. Manag.* **240**(1–3), 42–60 (2007), http://dx.doi.org/10.1016/j.foreco.2006.12.015.
16. S. M. Kercher, C. B. Frieswyk, and J. B. Zedler, "Effect of sampling teams and estimation methods on the assessment of plant cover," *J. Veg. Sci.* **14**(6), 899–906 (2003), http://dx.doi.org/10.1111/j.1654-1103.2003.tb02223.x.
17. A. Wright, A. Marcus, and R. Aspinall, "Evaluation of multispectral, fine scale digital imagery as a tool for mapping stream morphology," *Geomorphology* **33**(1–2), 107–120 (2000), http://dx.doi.org/10.1016/S0169-555X(99)00117-8.
18. R. G. Bryant and D. J. Gilvear, "Quantifying geomorphic and riparian land cover changes either side of a large flood event using airborne remote sensing: River Tay, Scotland," *Geomorphology* **29**(3–4), 307–321 (1999), http://dx.doi.org/10.1016/S0169-555X(99)00023-9.
19. R. G. Congalton et al., "Evaluating remotely sensed techniques for mapping riparian vegetation," *Comput. Electron. Agr.* **37**(1–3), 113–126 (2002), http://dx.doi.org/10.1016/S0168-1699(02)00108-4.
20. R. Dowling and A. Accad, "Vegetation classification of the riparian zone along the Brisbane River, Queensland, Australia, using light detection and ranging (lidar) data and forward looking digital video," *Can. J. Remote Sens.* **29**(5), 556–563 (2003), http://dx.doi.org/10.5589/m03-029.
21. S. J. Winterbottom and D. J. Gilvear, "A GIS-based approach to mapping probabilities of river bank erosion: regulated River Tummel, Scotland," *Regul. River.* **16**(2), 127–140 (2000), http://dx.doi.org/10.1002/(ISSN)1099-1646.
22. M. Kumma et al., "Riverbank changes along the Mekong River: remote sensing detection in the Vientiane-Nong Khai area," *Quatern. Int.* **186**(1), 100–112 (2008), http://dx.doi.org/10.1016/j.quaint.2007.10.015.

23. K. Johansen et al., "Quantifying indicators of riparian condition in Australian tropical savannas: integrating high spatial resolution imagery and field survey data," *Int. J. Remote Sens.* **29**(23), 7003–7028 (2008), http://dx.doi.org/10.1080/01431160802220201.
24. M. A. Lefsky et al., "LiDAR remote sensing for ecosystem studies," *Bioscience* **52**(1), 19–30 (2002), http://dx.doi.org/10.1641/0006-3568(2002)052[0019:LRSFES]2.0.CO;2.
25. C. Mallet and F. Bretar, "Full-waveform topographic lidar: state-of-the-art," *ISPRS J. Photogramm.* **64**(1), 1–16 (2009), http://dx.doi.org/10.1016/j.isprsjprs.2008.09.007.
26. D. J. Milan et al., "Filtering spatial error from DEMs: implications for morphological change estimation," *Geomorphology* **125**(1), 160–171 (2011), http://dx.doi.org/10.1016/j.geomorph.2010.09.012.
27. M. E. Charlton, A. R. G. Large, and I. C. Fuller, "Application of airborne LiDAR in river environments: the River Coquet, Northumberland, UK," *Earth Surf. Process.* **28**(3), 299–306 (2003), http://dx.doi.org/10.1002/(ISSN)1096-9837.
28. J. R. French, "Airborne LiDAR in support of geomorphological and hydraulic modeling," *Earth Surf. Process.* **28**(3), 321–335 (2003), http://dx.doi.org/10.1002/(ISSN)1096-9837.
29. B. Notebaert et al., "Qualitative and quantitative applications of LiDAR imagery in fluvial geomorphology," *Earth Surf. Process.* **34**(2), 217–231 (2009), http://dx.doi.org/10.1002/esp.v34:2.
30. L. M. G. Pereira and R. J. Wicherson, "Suitability of laser data for deriving geographical information: a case study in the context of management of fluvial zones," *ISPRS J. Photogramm.* **54**(2–3), 105–114 (1999), http://dx.doi.org/10.1016/S0924-2716(99)00007-6.
31. D. P. Thoma et al., "Airborne laser scanning for riverbank erosion assessment," *Remote Sens. Environ.* **95**(4), 493–501 (2005), http://dx.doi.org/10.1016/j.rse.2005.01.012.
32. A. Casas et al., "Assessing levee stability with geometric parameters derived from airborne LiDAR," *Remote Sens. Environ.* **117**, 281–288 (2012), http://dx.doi.org/10.1016/j.rse.2011.10.003.
33. P. Tarolli, G. Sofia, and G. D. Fontana, "Geomorphic features extraction from high-resolution topography: landslide crowns and bank erosion," *Nat. Hazards* **61**(1), 65–83 (2012), http://dx.doi.org/10.1007/s11069-010-9695-2.
34. L. A. Arroyo et al., "Integration of LiDAR and QuickBird imagery for mapping riparian biophysical parameters and land cover types in Australian tropical savannas," *Forest Ecol. Manag.* **259**(3), 598–606 (2010), http://dx.doi.org/10.1016/j.foreco.2009.11.018.
35. R. K. Hall et al., "Quantifying structural physical habitat attributes using LiDAR and hyperspectral imagery," *Environ. Monit. Assess.* **159**(1–4), 63–83 (2009), http://dx.doi.org/10.1007/s10661-008-0613-y.
36. J. R. Grove, J. Croke, and C. Thompson, "Quantifying different riverbank erosion processes during an extreme flood event," *Earth Surf. Process.* **38**(12), 1393–1406 (2013), http://dx.doi.org/10.1002/esp.3386.
37. C. Thompson and J. Croke, "Geomorphic effects, flood power, and channel competence of a catastrophic flood in confined and unconfined reaches of the upper Lockyer valley, southeast Queensland, Australia," *Geomorphology* **197**, 156–169 (2013), http://dx.doi.org/10.1016/j.geomorph.2013.05.006.
38. A. Simon and M. Rinaldi, "Disturbance, stream incision, and channel evolution: the roles of excess transport capacity and boundary materials in controlling channel response," *Geomorphology* **79**(3–4), 361–383 (2006), http://dx.doi.org/10.1016/j.geomorph.2006.06.037.
39. B. L. Finlayson and T. A. McMahon, "Australia vs the world: a comparative analysis of streamflow characteristics," in *Fluvial Geomorphology of Australia*, R. J. Warner, Ed., pp 17–40, Academic Press, Sydney (1988).
40. S. Ikeda, G. Parker, and K. Sawai, "Bend theory of river meanders. Part 1. Linear development," *J. Fluid Mech.* **112**, 363–377 (1981), http://dx.doi.org/10.1017/S0022112081000451.
41. S. Goetz, "Remote sensing of riparian buffers: past progress and future prospects," *J. Am. Water Resour. Assoc.* **42**(1), 133–143 (2006), http://dx.doi.org/10.1111/jawr.2006.42.issue-1.
42. P. S. Roberts, *Explanatory Notes on Baccus Marsh and Ballan 1:50,000 Geological Maps*, Geological Survery Report 76, Department of Minerals and Energy, Melbourne, Victoria (1984).
43. Melbourne Water, *Rivers and creeks* (2013), http://www.melbwater.com.au/content/rivers_and_creeks/river_health/werribee_waterways.asp?bhcp=1 (accessed 17 March 2013).

44. BoM (Bureau of Meteorology), *Climate Data Online*, www.bom.gov.au/climate/data/ (13 March 2013).
45. Victorian Water Resources Data Warehouse, *Victorian Rivers*, http://www.vicwaterdata.net/vicwaterdata/data_warehouse_content.aspx?option=5 (17 March 2013).
46. K. Johansen et al., "Mapping riparian condition indicators in a sub-tropical savanna environment from discrete return LiDAR data using object-based image analysis," *Ecol. Indic.* **10**(4), 796–807 (2010), http://dx.doi.org/10.1016/j.ecolind.2010.01.001.
47. K. Johansen, M. Hewson, and S. Phinn, *Pilot Project: Assessing Riparian Vegetation and Physical Form Using Remote Sensing*, Department of Sustainability and Environment, Melbourne, Victoria (2008).
48. L. Klimes, "Scale-dependent variation in visual estimates of grassland plant cover," *J. Veg. Sci.* **14**(6), 815–821 (2003), http://dx.doi.org/10.1111/j.1654-1103.2003.tb02214.x.
49. C. R. Hupp et al., "Bank erosion along the dam-regulated lower Roanoke River, North Carolina," in *Management and Restoration of Fluvial Systems with Broad Historical Changes and Human Impacts*, L. A. James, S. I. Rathburn, and G. R. Whittecar, Eds., Geological Society of America Special Paper 451, pp. 97–108 (2009).
50. C. R. Thorne, "Processes, and mechanisms of river bank erosion," in *Gravel Bed Rivers*, R. D. Hey, J. C. Bathurst, and C. R. Thorne, Eds., pp. 227–259, Wiley, Chichester (1982).
51. P. Scarth, J. Armston, and T. Danaher, "On the relationship between crown cover, foliage projective cover and leaf area index," in *14th Australasian Remote Sensing and Photogrammetry Conference*, R. Bartolo and A. Edwards, Spatial Sciences Institute, Australia (2008).
52. J. L. Lovell et al., "Using airborne and ground-based ranging lidar to measure canopy structure in Australian forests," *Can. J. Remote Sens.* **29**(5), 607–622 (2003), http://dx.doi.org/10.5589/m03-026.
53. J. D. Armston et al., "Prediction and validation of foliage projective cover from Landsat-5 TM and Landsat-7 ETM+ imagery for Queensland, Australia," *J. Appl. Remote Sens.* **3**(1), 033540 (2009), http://dx.doi.org/10.1117/1.3216031.
54. T. Blaschke, "Object based image analysis for remote sensing," *ISPRS J. Photogramm.* **65**(1), 2–16 (2010), http://dx.doi.org/10.1016/j.isprsjprs.2009.06.004.
55. U. C. Benz et al., "Multi-resolution, object-oriented fuzzy analysis of remote sensing data for GIS-ready information," *ISPRS J. Photogramm.* **58**(3–4), 239–258 (2004), http://dx.doi.org/10.1016/j.isprsjprs.2003.10.002.
56. K. Johansen et al., "Automatic geographic object based mapping of streambed and riparian zone extent from LiDAR data in a temperate rural urban environment, Australia," *Remote Sens.* **3**(6), 1139–1156 (2011), http://dx.doi.org/10.3390/rs3061139.
57. G. Pickup, V. H. Chewings, and D. J. Nelson, "Estimating changes in vegetation cover over time in arid rangelands using Landsat MSS data," *Remote Sens. Environ.* **43**(3), 243–263 (1993), http://dx.doi.org/10.1016/0034-4257(93)90069-A.
58. G. N. Bastin, R. W. Tynan, and V. H. Chewings, "Implementing satellite-based grazing gradient methods for rangeland assessment in South Australia," *Rangeland J.* **20**(1), 61–76 (1998), http://dx.doi.org/10.1071/RJ9980061.
59. J. A. Ludwig et al., "A new landscape leakiness index based on remotely sensed ground-cover data," *Ecol. Indic.* **6**(2), 327–336 (2006), http://dx.doi.org/10.1016/j.ecolind.2005.03.010.
60. G. Pickup, G. N. Bastin, and V. H. Chewings, "Measuring rangeland vegetation with high resolution airborne videography in the blue-near infrared spectral region," *Int. J. Remote Sens.* **21**(2), 339–351 (2000), http://dx.doi.org/10.1080/014311600210867.
61. R Development Core Team, *R: A Language and Environment for Statistical Computing*, R Foundation for Statistical Computing, Vienna, Austria (2007).
62. A. Agresti, *Categorical Data Analysis*, 2nd ed., John Wiley and Sons, Inc., Hoboken, New Jersey (2002).
63. E. T. Harrison, R. H. Norris, and S. N. Wilkinson, "Can an indicator of river health be related to assessments from a catchment-scale sediment model?," *Hydrobiologia* **600**(1), 49–64 (2008), http://dx.doi.org/10.1007/s10750-007-9175-1.
64. B. Abernethy and I. D. Rutherfurd, "The distribution and strength of riparian tree roots in relation to riverbank reinforcement," *Hydrol. Process.* **15**(1), 63–79 (2001), http://dx.doi.org/10.1002/(ISSN)1099-1085.

65. D. M. Lawler, "The impact of scale on the processes of channel-side sediment supply: a conceptual model," in *Effects of Scale on the Interpretation and Management of Sediment and Water Quality*, W. R. Ostercamp, Ed., Vol. 226, pp 175–185, IAHS Press, Wallingford (1995).
66. J. Oksanen and T. Sarjakoski, "Error propagation of DEM-based surface derivatives," *Comput. Geosci.* **31**(8), 1015–1027 (2005), http://dx.doi.org/10.1016/j.cageo.2005.02.014.
67. N. R. Goodwin, N. C. Coops, and D. S. Culvenor, "Assessment of forest structure with airborne LiDAR and the effects of platform altitude," *Remote Sens. Environ.* **103**(2), 140–152 (2006), http://dx.doi.org/10.1016/j.rse.2006.03.003.
68. T. Takahashi, K. Yamanoto, and S. M. Tsuzuku, "Estimating individual tree heights of sugi (Cryptomeria japonica D. Don) plantations in mountaninous areas using small-footprint airborne LiDAR," *J. For. Res.* **10**(2), 135–142 (2005), http://dx.doi.org/10.1007/s10310-004-0125-8.
69. K. Fryirs, B. Chessman, and I. Rutherfurd, "Progress, problems and prospects in Australian river repair," *Mar. Freshwater Res.* **64**, 642–654 (2013), http://dx.doi.org/10.1071/MF12355.

Kasper Johansen is a research fellow in the School of Geography, planning and environmental management at the University of Queensland. His primary contribution has been the development of operational approaches at multiple spatial scales for riparian zone mapping and monitoring in different Australian environments using high spatial resolution image data as a tool for replacing more conventional and time-consuming field based methods. Dr. Johansen's main research focus is on the analysis of high spatial resolution image datasets, including satellite and airborne image and LiDAR data, with emphasis on specialized techniques such as geographic object-based image analysis and innovative approaches for integrating field survey data of biophysical variables with high spatial resolution image data. Dr. Johansen has also coordinated a large number of field and airborne campaigns for collecting field and high spatial resolution airborne hyper-spectral and LiDAR data.

James Grove is an honorary research fellow in the Department of Resource Management and Geography at the University of Melbourne. He is a fluvial geomorphologist with a research focus on riverbank erosion rates and processes at the catchment scale. The use of field measurements to quantify riverbank erosion has recently been integrated with LiDAR data from pre and post floods to provide volumes of erosion and deposition. The determination of processes has also been applied to geomorphic river condition assessment at a state scale in Victoria and Tasmania, Australia, and the effects of regulation on riverbank erosion processes downstream of dams. To assist with these pieces of research the EcoEvidence tool has been used to quantify the geomorphic data that underpins decision making in river management. He has also conducted research in Spitzbergen on the sub-arctic river slush flows, and in Greenland and Iceland on glacial river flows and sediment dynamics.

Robert Denham is an environmental statistician in the Remote Sensing Centre of Queensland Department of Science, Information Technology, Innovation and the Arts. Robert's main interests are developing statistical methods for linking vegetation characteristics to remotely sensed data. Currently he is involved with image time series methods to describe temporal changes in woody vegetation structure. Dr. Denham also works on land use classification and evaluation and is currently leading a DSITIA project to produce historical crop maps using Landsat imagery. Other interests include Bayesian statistical analysis, particularly of image time series data.

Stuart Phinn is professor of Geography in the School of Geography, Planning and Environmental Management at the University of Queensland. He is also the director of the Biophysical Remote Sensing Group and Joint Remote Sensing Research Program at the University of Queensland. Prof. Phinn graduated with a PhD in geography from the joint doctoral program between San Diego State University and the University of California at Santa Barbara in 1997. Since that time he has worked in teaching and research academic positions covering remote sensing in Australia and internationally. His work focuses on understanding changes to the environment using information collected from satellites and aircraft sensors and in developing more collaborative approaches to ecosystem science and management.